Jiang *et al. Microstructures* **2025**, *5*, 2025009
DOI: 10.20517/microstructures.2023.100

Microstructures

Research Article

Open Access

Tunable type-I band alignment and electronic structure of GaSe/$MoSi_2N_4$ van der Waals heterostructure

Hongxing Jiang[#], Xiangjiu Zhu[#], Dandan Wang, Lihua Yang, Yang Liu, Xin Qu, Huilian Liu

Key Laboratory of Functional Materials Physics and Chemistry of the Ministry of Education, Key Laboratory of Preparation and Application of Environmental Friendly Materials, College of Physics, Jilin Normal University, Changchun 130103, Jilin, China.
#Authors contributed equally.

Correspondence to: Dr. Xin Qu and Dr. Huilian Liu, Key Laboratory of Functional Materials Physics and Chemistry of the Ministry of Education, Key Laboratory of Preparation and Application of Environmental Friendly Materials, College of Physics, Jilin Normal University, 399 Zhuoyue Street, Hi-tech Development Zone, Changchun 130103, Jilin, China. E-mail: quxin515@163.com; lhl541@126.com

How to cite this article: Jiang, H.; Zhu, X.; Wang, D.; Yang, L.; Liu, Y.; Qu, X.; Liu, H. Tunable type-I band alignment and electronic structure of GaSe/$MoSi_2N_4$ van der Waals heterostructure. *Microstructures* **2025**, *5*, 2025009. https://dx.doi.org/10.20517/microstructures.2023.100

Received: 26 Dec 2023 **First Decision:** 23 Feb 2024 **Revised:** 22 Mar 2024 **Accepted:** 4 Dec 2024 **Published:** 24 Jan 2025

Academic Editors: Yi Du, Liangzhi Kou **Copy Editor:** Ping Zhang **Production Editor:** Ping Zhang

Abstract

In this study, we have conducted an investigation on the structural characteristics and electronic properties of van der Waals heterostructures (vdWHs) composed of Gallium selenide (GaSe) and $MoSi_2N_4$. The analysis was carried out using first-principles methods. The findings indicate that the heterostructure exhibits stability at standard room temperature and possesses characteristics of an indirect bandgap semiconductor. Interestingly, we observed that the band edges of the heterostructure of monolayer GaSe and $MoSi_2N_4$ were able to form a type-I band alignment. Therefore, in the field of optoelectronic devices, GaSe/$MoSi_2N_4$ vdWHs can be widely used in light-emitting devices such as diodes. In addition, through the application of an external electric field and in-plane strain, the band edges of GaSe/$MoSi_2N_4$ vdWHs can be separated from the GaSe and $MoSi_2N_4$ layers, forming a transition from the type-I to type-II band alignment, which is very favorable for realizing effective electron-hole separation. Therefore, GaSe/$MoSi_2N_4$ vdWHs have great potential as an adjustable material in optoelectronic applications.

Keywords: Two-dimensional heterostructures, first-principles calculations, electronic properties

© The Author(s) 2025. **Open Access** This article is licensed under a Creative Commons Attribution 4.0 International License (https://creativecommons.org/licenses/by/4.0/), which permits unrestricted use, sharing, adaptation, distribution and reproduction in any medium or format, for any purpose, even commercially, as long as you give appropriate credit to the original author(s) and the source, provide a link to the Creative Commons license, and indicate if changes were made.

INTRODUCTION

Van der Waals heterostructures[1-4] (vdWHs) are stacked structures made of atomically two-dimensional (2D) layered materials. Such structures are of intense interest to the scientific community because these structures may integrate 2D materials[5,6] with varied properties at the atomic scale, thereby offering a standard platform for applications in electronics and optoelectronics. Using van der Waals forces, it is possible to construct structures with specific functions by stacking various 2D monolayers of materials. Researchers are able to govern the interface and electronic characteristics of materials by modifying the stacking order of different materials thanks to the adaptability of this structure, which enables various applications[7-9]. The band alignment (When the band alignment appears below, it is denoted by the abbreviation b-a) of heterostructures is a crucial characteristic that can be categorized into three distinct types: straddling type-I, staggered type-II, and broken-gap type-III. Each specific b-a is associated with certain applications for electronic devices. Type-I b-a is advantageous for spatially restricting electrons and holes, which allows for more effective recombination to be achieved; optical device applications benefit from type-I b-a[10,11]. In contrast to type-I b-a, type-III b-a engineering facilitates the transition of energy between the conduction band and the valence band. Consequently, type-III b-a holds a unique potential for use in photodetectors and tunnel field effect transistors[12,13]. However, for type-II b-a, it is evident that the shifting of bands facilitates the separation of carriers, which is ideal for attaining efficient electron-hole separation and thus proves advantageous for applications involving electronic devices and photocatalysis[14,15]. Much research has been done on 2D layered materials and vdWHs because of these worthwhile applications.

Gallium selenide (GaSe) is a widely studied layered structure that has garnered significant interest in the fields of optoelectronics, terahertz radiation detection, and nonlinear optics[16]. The crystal structure of GaSe is hexagonal with the space group P-3m1. In recent times, there have been successful endeavors to extract high-quality single and few-layer GaSe nanosheets using different methods, including chemical and mechanical exfoliation, as well as vapor phase deposition or epitaxy growth[17,18]. The 2D GaSe nanosheets exhibit a remarkable on-off current ratio of approximately 10^5, together with a significantly high photoresponsivity of up to 2.8 A W^{-1}. This photoresponsivity surpasses that of MoS_2 and graphene[17,19]. Recent theoretical and experimental investigations have demonstrated that the monolayer form of GaSe exhibits promising characteristics as a potential photocatalyst[20,21]. Nevertheless, the significant experimental bandgap range of 3-3.5 eV could potentially impede the practical implementation of this material as a promising photocatalyst, primarily due to its limited ability to effectively utilize visible light[22,23]. Moreover, it has been experimentally verified that the bulk carrier mobility of GaSe is 215 cm^2 V^{-1} s^{-1}, and there is potential for a substantial increase in mobility when GaSe is reduced to a few layers[24]. The acquisition of single-layer GaSe represents a significant advancement in the realm of 2D materials, thereby broadening the scope of this material family. This development also paves the way for novel opportunities in the field of optoelectronic device applications[25-30].

Recently, the successful fabrication of a $MoSi_2N_4$ monolayer has been achieved by the process of chemical vapor deposition[31]. Using first-principles calculations, Hong *et al.*[31] were able to make a prediction regarding the electronic properties of the $MoSi_2N_4$ monolayer. Specifically, they determined that this monolayer possesses the characteristics of a direct bandgap semiconductor. The calculated bandgap value, acquired using the Perdew, Burke, and Ernzerhof (PBE)/Heyd-Scuseria-Ernzerhof (HSE06) method, was found to be 1.744/2.297 eV. Theoretical investigations have been conducted to examine the electrical and optical characteristics of the $MoSi_2N_4$ monolayer[32-34]. The investigation of contact heterostructures using $MoSi_2N_4$ and various 2D and 3D materials has been conducted. Examples of such heterostructures include $MoSi_2N_4$/graphene[35,36], $MoSi_2N_4/MoS(Se)_2$[37,38], and $MoSi_2N_4$/metals[39]. The electrical and optical properties

of the $MoSi_2N_4$ monolayer are significantly influenced when it comes into contact with other 2D materials. Cai *et al*.[38] conducted a study on the construction of the $MoSi_2N_4$/$MoSe_2$ vdWH. Their findings indicate that the $MoSi_2N_4$/$MoSe_2$ vdWHs exhibit a type-I b-a, resulting in improved optical absorption and carrier mobility when compared to the individual monolayers.

Tunable b-a and electronic properties of GaSe/$MoSi_2N_4$ vdWHs have not been studied to date. The objective of this investigation is to perform first-principles research on the electronic structure of GaSe/$MoSi_2N_4$ vdWHs. In addition, we explored the potential to adjust its b-a through the application of interlayer distance, biaxial strain, and applied electric fields. The results show that the GaSe/$MoSi_2N_4$ vdWHs exhibit stability under ambient conditions and possess characteristics of an indirect bandgap semiconductor. Furthermore, it was observed that the band edges of the heterostructure, which consists of a monolayer of GaSe and $MoSi_2N_4$, exhibit type-I b-a. Through the control of biaxial strain and the action of applied electric field, the direction type of the band can be effectively adjusted from type-I to type-II. This adjustment facilitates the efficient separation of electrons and holes that are created. Our results show that the GaSe/$MoSi_2N_4$ vdWH has good properties as a multifunctional material and has great potential in the field of optoelectronics.

COMPUTATIONAL METHODS

This study presents the outcomes of our investigation into the geometric optimization, electrical structures, and b-a of the GaSe/$MoSi_2N_4$ vdWHs, employing first-principles calculations. The density functional theory framework[40] is utilized for structure optimization and property computations. These calculations are performed using the standard version of Vienna ab initio simulation package (VASP.5.4.4)[41], which employs the projector-augmented plane wave (PAW) approach[42] to account for the ion-electron interaction. The software program known as Visualisation for Electronic Structural Analysis (VESTA)[43] is widely employed for the manipulation and analysis of various forms of data pertaining to structural models, volumetric data encompassing electron and nuclear densities, and crystal morphologies. The electronic exchange-correlation functional is addressed in this study by employing the generalized gradient approximation (GGA)[44] as determined by PBE[45]. The energy cutoff of the plane waves is established at 550 eV with an energy accuracy of 10^{-6} eV, and the k-point mesh of the Brillouin zone is set to be 8 × 8 × 1. The atomic locations undergo complete relaxation until the magnitude of the force acting on each atom is below 10^{-3} eV/Å. The supercell technique is commonly employed for simulating monolayers, wherein a vacuum separation of around ~40 Å is employed to mitigate the interaction between neighboring layers. Given that the GGA tends to underestimate bandgaps, we employ the HSE06 hybrid functional[46] for the computation of band structures. The computation of dynamic stabilities and phonon dispersion curves is carried out using the supercell technique, which is implemented in the Phonopy code[47]. The inclusion of the dipole correction was also accounted for in the calculations.

RESULTS AND DISCUSSION

Figure 1 shows the atomic structure, phonon spectrum, projected band structure and state density of semiconductor GaSe and $MoSi_2N_4$ monolayers. After geometric optimization, both GaSe (γ' phase, in these papers as 1T phase)[48] and $MoSi_2N_4$ (1T, 2H) showed layered atomic structures with lattice constants of 3.64 Å, 2.90 Å and 2.89 Å. As illustrated in Figure 1A-C, for the optimized GaSe geometry, it is observed that the Ga atom is connected to two Se atoms, while in the $MoSi_2N_4$ geometry, the Mo-N_2 layer is situated in between the Si-N double layer. By calculating the band structure of the GaSe monolayer through HSE06 and PBE, it can be found in Figure 1G and J that GaSe has semiconductor characteristics and is an indirect bandgap semiconductor. The locations of the conduction band minimum (CBM) and valence band maximum (VBM) are identified to be at the M and Γ points. The PBE and HSE06 approaches both

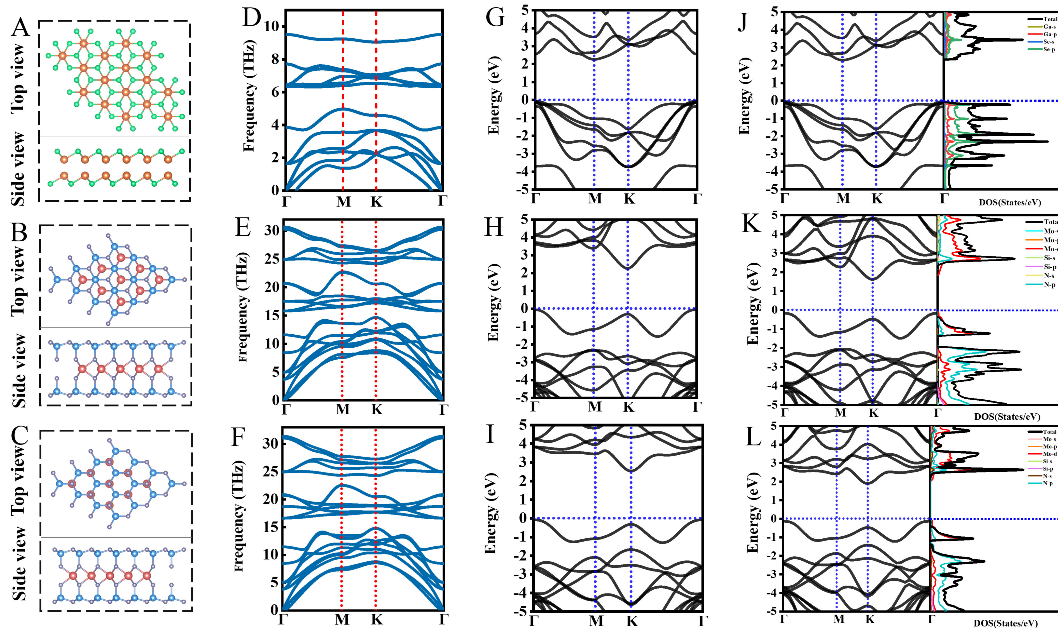

Figure 1. (A-C) Shows the optimized atomic structure, phonon dispersion curve (D-F); (G-I) HSE06 projected band structure and state density are 1T-GaSe, 1T-$MoSi_2N_4$, 2H-$MoSi_2N_4$; (J-L) are the PBE projected band structure and state density of 1T-GaSe, 1T-$MoSi_2N_4$, 2H-$MoSi_2N_4$. The green, orange, red, blue, and silver spheres represent selenium, gallium, molybdenum, silicon, and nitrogen atoms. HES06: Heyd-scuseria-ernzerhof; GaSe: Gallium selenid; PBE: Perdew, burke, and ernzerhof.

anticipate the identical features of the GaSe monolayer, with a bandgap value of 2.32 eV for each calculation method. The contribution of the atoms in the GaSe monolayer is shown in Figure 1J. The red and green lines correspond to the respective contributions made by gallium and selenium atoms. It is shown that both VBM and CBM of GaSe monolayers are predominantly contributed by the p-orbital of Se atoms. Figure 1D illustrates the phonon spectrum of the monolayer GaSe. The figure illustrates that the frequency of the 2D GaSe monolayer is positive and there is an absence of virtual frequency, so indicating the dynamic stability of the material.

Additionally, the $MoSi_2N_4$ monolayer is also an indirect bandgap semiconductor, and the CBM and VBM of 1T- $MoSi_2N_4$ and 2H- $MoSi_2N_4$ are located at the K and Γ points. In the ground state, the band structures of 1T-$MoSi_2N_4$ and 2H-$MoSi_2N_4$ monolayers were calculated by HSE06 and PBE [Figure 1H, I, K and L]. The bandgap values obtained by HSE06 methods are 2.38 eV and 2.61eV, and those obtained by PBE methods are 1.81 eV and 2.02 eV. It is imperative to acknowledge that conventional PBE techniques frequently underestimate the bandgap of 2D semiconductors. To address this limitation, the HSE06 approach can be employed to acquire a more precise and reliable bandgap. However, the bandgap measurement of the $MoSi_2N_4$ monolayer in the experiment yielded a value of 1.94 eV[31], which is in greater agreement with our PBE calculation. Therefore, we used the PBE method for subsequent related calculations. Furthermore, we found that the bandgap of 1T-$MoSi_2N_4$ is closer to the experimental value compared to that of 2H-$MoSi_2N_4$. Meanwhile, the total energy of 1T-$MoSi_2N_4$ is lower than that of 2H-$MoSi_2N_4$. Hence, we will further investigate the correlated electronic properties of the vdWH formed by monolayers of 1T-$MoSi_2N_4$ and 1T-GaSe in the following sections. The contribution of atoms in the monolayer of $MoSi_2N_4$ is shown in Figure 1K and L. The red and blue lines represent the contributions of molybdenum and nitrogen atoms. This suggests that the p-orbital of the N atom contributes most to the VBM of the $MoSi_2N_4$ monolayer, while the d-orbital of the Mo atom contributes most to the CBM. The phonon spectrum of the $MoSi_2N_4$ monolayer is shown in Figure 1E and F, illustrating that the frequency of the 2D $MoSi_2N_4$ monolayer is

positive, indicating its dynamic stability. Additionally, there is no presence of virtual frequency, further supporting its stability.

GaSe/$MoSi_2N_4$ vdWHs can be obtained by stacking the GaSe monolayer in the z direction on top of the $MoSi_2N_4$ monolayer. The initial equilibrium layer spacing D is set to 3.39 Å, which is larger than the sum of covalent radii between Se and N atoms, thus providing evidence that there is no formation of a covalent bond between the two constituent monolayers. Due to the difference in lattice parameters between GaSe and $MoSi_2N_4$ monolayers, we use a supercell composed of (√3 × √3) GaSe and (2 × 2) $MoSi_2N_4$. Additionally, we consider three potential stack configurations, AA-stacking, AB-stacking and AC-stacking modes, which correspond to Figure 2A-C. As illustrated in Figure 2, in the AA-stacking configuration, Se atoms correspond to Mo atoms; in the AB-stacking configuration, Se atoms are in the center of Mo and Si atoms, and in the AC-stacking configuration, Si atoms correspond to Se atoms at the center point. The calculation results show that the energy in Figure 2C is relatively low (E_b about -7.26972 eV). Because the lattice parameters of GaSe and $MoSi_2N_4$ monolayers are different, we use a supercell composed of (√3 × √3) GaSe and (2 × 2) $MoSi_2N_4$. Based on m-n/m+n < 5% (m, n is the lattice constant of monolayer GaSe and $MoSi_2N_4$), the lattice parameter of the combination of GaSe/$MoSi_2N_4$ is 6.30 Å, resulting in a lattice mismatch rate of 4.1% < 5%, which proves the rationality of the heterostructure. Furthermore, to assess the stability of the structure, we determined the binding energy using $E_b = E_{vdWHs} - E_{GaSe} - E_{M_0si_2N_4}$, where E_{vdWHs}, E_{GaSe} and $E_{M_0si_2N_4}$ are the total energy of the corresponding vdWHs and GaSe and $MoSi_2N_4$ monolayer. The binding energy of GaSe/$MoSi_2N_4$ is -2.19 eV. The binding energy of vdWHs is negative, indicating that their energy is stable. In order to assess the mechanical stability of GaSe/$MoSi_2N_4$ vdWHs, we additionally computed the elastic constants. The elastic constants C_{11}, C_{12} and $C_{66} = (C_{11} - C_{12})/2$ of GaSe/$MoSi_2N_4$ vdWHs are calculated as 387 N/m, 90 N/m and 148 N/m. The Born-Huang criterion[49,50] suggests that the elastic constants $C_{11} > C_{12}$ and $C_{66} > 0$ of vdWHs demonstrate stability. We also calculate Young's modulus and Poisson's ratio of $Y = (C_{11}^2 - C_{12}^2)/C_{11}$, $V = C_{12}/C_{11}$ and other systems. The Supplementary Figure 1 describes the orientation-dependent Young's modulus and Poisson's ratio of vdWHs, showing that the Young's modulus and Poisson's ratio of GaSe/$MoSi_2N_4$ is isotropic. The average Young's modulus of GaSe/$MoSi_2N_4$ vdWHs is 366 N/m and Poisson's ratio is 0.23. The results show that the vdWHs have high in-plane stiffness. Additionally, another key factor is the stability at high temperatures. Ab initio molecular dynamics (AIMD) simulations were performed to investigate the thermal stability of the heterostructure. The results of the energy fluctuations over 20 ps, along with the final snapshot, are presented in Supplementary Figure 2. The GaSe/$MoSi_2N_4$ heterostructure maintained structural integrity and stable energy at temperatures up to 1000 K. The well-preserved geometric structure suggests that the GaSe/$MoSi_2N_4$ heterostructure may have practical applications even under high-temperature conditions.

Figure 3A and B Depicts the band structure of GaSe/$MoSi_2N_4$ vdWHs. The band structure calculated by PBE and HSE06 methods shows that GaSe/$MoSi_2N_4$ vdWHs demonstrate characteristics of a semiconductor, with the CBM situated at the K point and the VBM situated at the Γ point. This suggests that GaSe/$MoSi_2N_4$ vdWHs are an indirect bandgap semiconductor. The band shape and b-a type of GaSe/$MoSi_2N_4$ vdWHs remain unchanged when utilizing the HSE calculation approach in contrast to the PBE method. Therefore, the PBE method can accurately predict the electronic structure of GaSe/$MoSi_2N_4$ vdWHs. Due to computational cost savings, we decided to use the PBE method for all subsequent calculations. In addition, according to the band structure diagram shown in Figure 3, we find that both VBM and CBM are contributed by the $MoSi_2N_4$ layer. Thus, GaSe/$MoSi_2N_4$ vdWHs form a type-I b-a.

In order to gain a deeper comprehension of the charge distribution within GaSe/$MoSi_2N_4$ vdWHs, the electron density difference is computed using[51,52]: $\Delta\rho = \rho_{vdWHs} - \rho_{GaSe} - \rho_{MoSi2N4}$, where ρ_{vdWHs}, ρ_{GaSe} and $\rho_{MoSi2N4}$

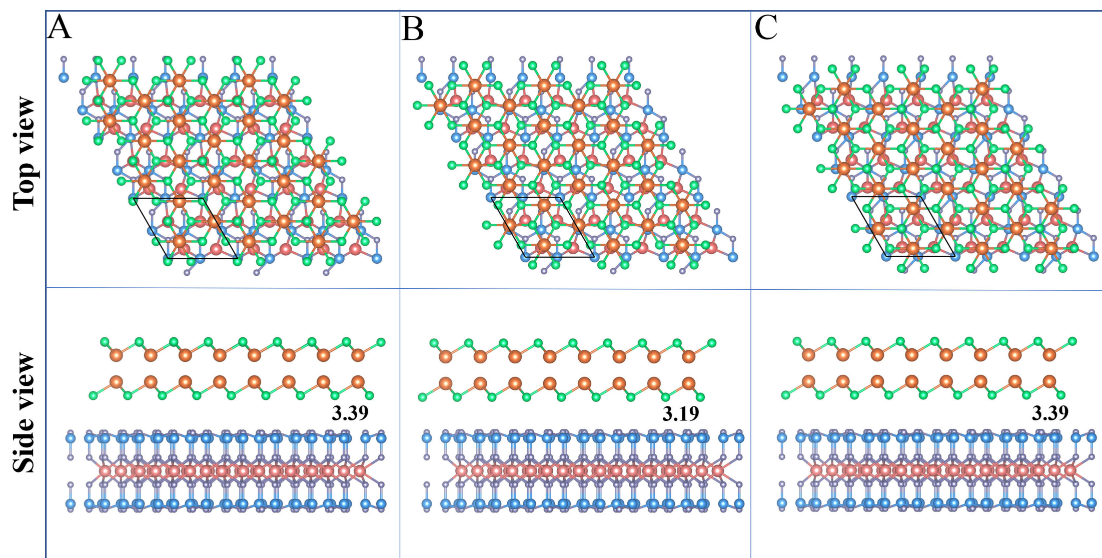

Figure 2. (A-C) Three different stacking forms of $GaSe/MoSi_2N_4$ vdWHs. The green, orange, red, blue, and silver spheres represent selenium, gallium, molybdenum, silicon, and nitrogen atoms. vdWHs: van der Waals heterostructures; GaSe: Gallium selenid; PBE: Perdew, burke, and ernzerhof; HES06: Heyd-scuseria-ernzerhof; CBM: Conduction band minimum; VBM: Valence band maximum.

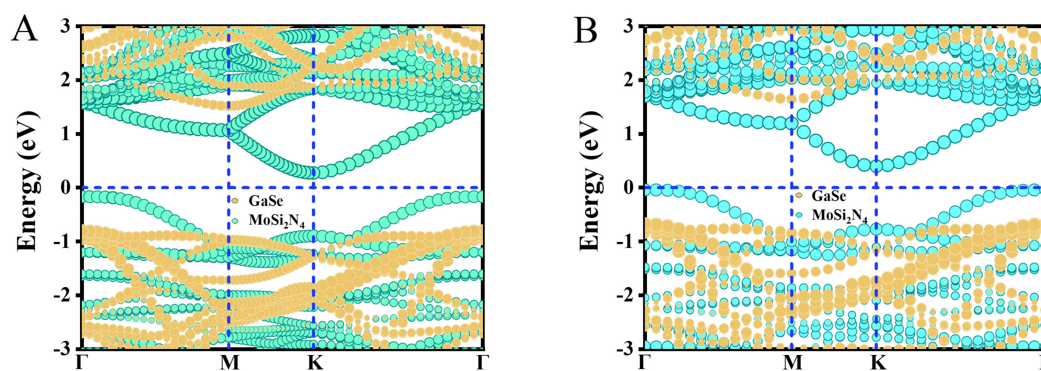

Figure 3. (A and B) Weighted projected band structures of $GaSe/MoSi_2N_4$ vdWHs calculated by PBE and HES06. vdWHs: van der Waals heterostructures; PBE: Perdew, burke, and ernzerhof; HES06: Heyd-scuseria-ernzerhof.

represent the charge density of $GaSe/MoSi_2N_4$ vdWHs, a single GaSe monolayer, and $MoSi_2N_4$ monolayer, respectively. Charge depletion is represented by the cyan zone and charge accumulation is represented by the yellow region. The electron redistribution that takes place at the contact surface is clearly depicted in Figure 4A. More specifically, the predominant concentration of charge distribution occurs at the interface between the GaSe monolayer and $MoSi_2N_4$, where electrons are consumed in the Ga-Se layer and accumulate in the Si-N layer. Thus, The charge transfer occurs from the GaSe layer to the $MoSi_2N_4$ layer. The electrostatic potential of $GaSe/MoSi_2N_4$ vdWHs is shown in Figure 4B and C. The $MoSi_2N_4$ layer exhibits a greater potential depth compared to the GaSe layer, leading to the establishment of a built-in electric field at the interface. To have a better understanding of the interface's charge redistribution, we further calculate the $GaSe/MoSi_2N_4$ vdWHs and the work function of the composition of the monolayer using:

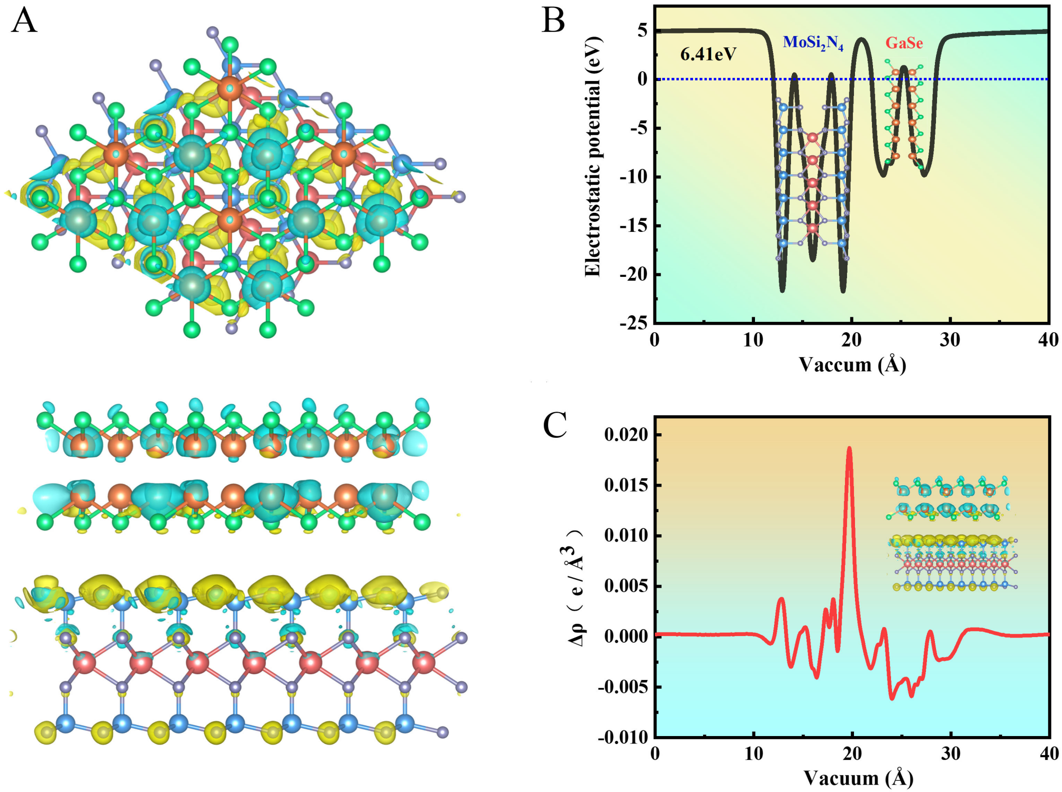

Figure 4. (A) In-plane average charge density difference of GaSe/$MoSi_2N_4$ vdWHs; (B and C) in-plane average electrostatic potential of GaSe/$MoSi_2N_4$ vdWHs. Inset represents the 3D charge density difference in the heterostructure. The yellow and cyan regions represent charge accumulation and depletion, respectively. vdWHs: van der Waals heterostructures; GaSe: Gallium selenide.

$$\Phi = E_{VAC} - E_F \tag{1}$$

Here, E_{VAC} and E_F stand for vacuum energy and Fermi energy, respectively. The calculated work functions of isolated GaSe and $MoSi_2N_4$ layers are 5.28 eV and 6.86 eV, while the work functions of GaSe/$MoSi_2N_4$ vdWHs are 6.41 eV. The work function of GaSe/$MoSi_2N_4$ vdWHs is shown in Figure 5. It is observed that the work function of single-layer $MoSi_2N_4$ is higher than that of GaSe/$MoSi_2N_4$ vdWHs, indicating that electrons accumulate on the $MoSi_2N_4$ side and are consumed on the GaSe side, both of which are transferred from GaSe to $MoSi_2N_4$. The observed direction of charge transfer aligns with the findings shown in Figure 4. The presence of the built-in electric field is attributed to the phenomenon of interfacial charge transfer. Hence, the mobility of carriers and the injection of charges may be influenced. Besides, to establish carrier migration, we calculate the effective mass in such vdWHs. Using VBM and CBM fitting for band edge dispersion, we calculate the effective mass of the electron (m_e*) and hole (m_h*) using

$$\frac{1}{m^*} = \frac{1}{\hbar} \times \frac{\partial^2 E(\boldsymbol{k})}{\partial \boldsymbol{k}^2} \tag{2}$$

In this context, E(k) represents the energy dispersion, $\hbar$denotes Planck's constant, and k represents the wave vector. The calculated electrons and holes of GaSe/$MoSi_2N_4$ vdWHs and the effective masses of the monolayer are listed in Table 1. It can be found that the calculated electron effective mass of GaSe/$MoSi_2N_4$ vdWHs is 0.38 m_0, which is still smaller than the value of GaSe and $MoSi_2N_4$ monolayer, thus indicating that GaSe/$MoSi_2N_4$ vdWHs has a higher carrier migration mobility. Furthermore, the carrier mobility of the

Table 1. Calculated lattice parameters (*a*), interlayer distance (*D*), bandgap (E_g), and contact type. Effective mass (*m*) and mobility (μ) along the x and y directions are obtained by PBE calculations

	a (Å)	*D* (Å)	*Eg* (eV)	Contact types	m_e^x/m_0	m_h^y/m_0	μ_x (10^2 cm^2 V^{-1} s^{-1})	μ_y (10^2 cm^2 V^{-1} s^{-1})
GaSe	3.64	-	2.32	-	0.43	0.75	5.32	9.17
1T-$MoSi_2N_4$	2.90	-	1.81	p-ShC	0.54	2.87	2.76	2.47
GaSe/$MoSi_2N_4$	6.30	3.40	0.44	p-ShC	0.38	5.19	3.27	4.89

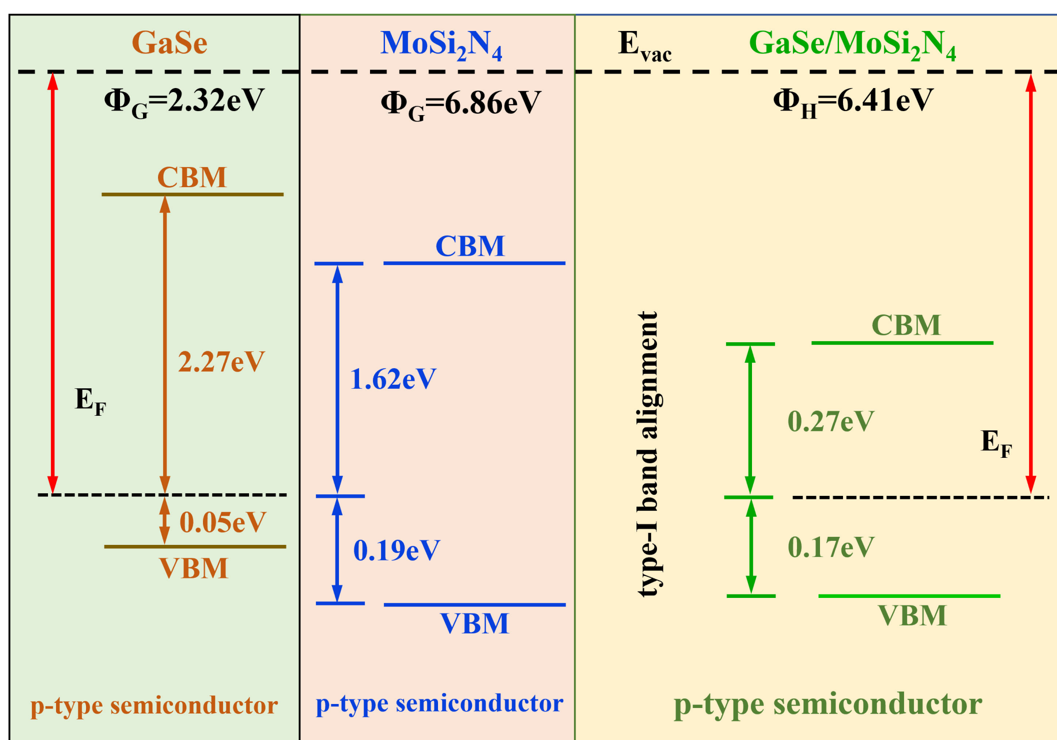

Figure 5. The work functions of GaSe, $MoSi_2N_4$ monolayer and their vdWHs. vdWHs: van der Waals heterostructures; GaSe: Gallium selenide.

GaSe/$MoSi_2N_4$ heterostructure calculated in this study (489 cm^2 V^{-1} s^{-1}) is slightly higher than that of MoS_2 (410 cm^2 V^{-1} s^{-1}), yet it is lower than that of silicon (1,400 cm^2 V^{-1} s^{-1}). These findings suggest that our work holds significant potential for applications in the field of optoelectronics.

It is commonly recognized that controlling mechanical strain can effectively control the physical characteristics of 2D materials. In this study, we investigate the impact of strain engineering on GaSe/$MoSi_2N_4$ vdWHs by adjusting the interlayer distance, as shown in Figure 6A. Notably, interlayer distance in 2D-based vdWHs can be controlled using scanning tunneling microscopy[53] or vacuum thermal annealing[54]. We also calculated three stacking modes of GaSe/$MoSi_2N_4$ vdWHs at different interlayer distances in Supplementary Table 1. The results show that AC-stacking in GaSe/$MoSi_2N_4$ vdWHs has the lowest binding energy. Here, the strain is applied by adjusting the interlayer distance, defined as $\Delta D = D - D_0$, where the value of the original D is 3.4 Å and D_0 is the interlayer distance after the strain. By increasing the interlayer distance D, the tensile strain is specified, and by reducing D, the compressive strain is defined. $\Delta D < 0$ indicates compressive strain, while $\Delta D > 0$ indicates tensile strain. As illustrated in Figure 6A, the bandgap of GaSe/$MoSi_2N_4$ vdWHs gradually increases as the interlayer distance gradually

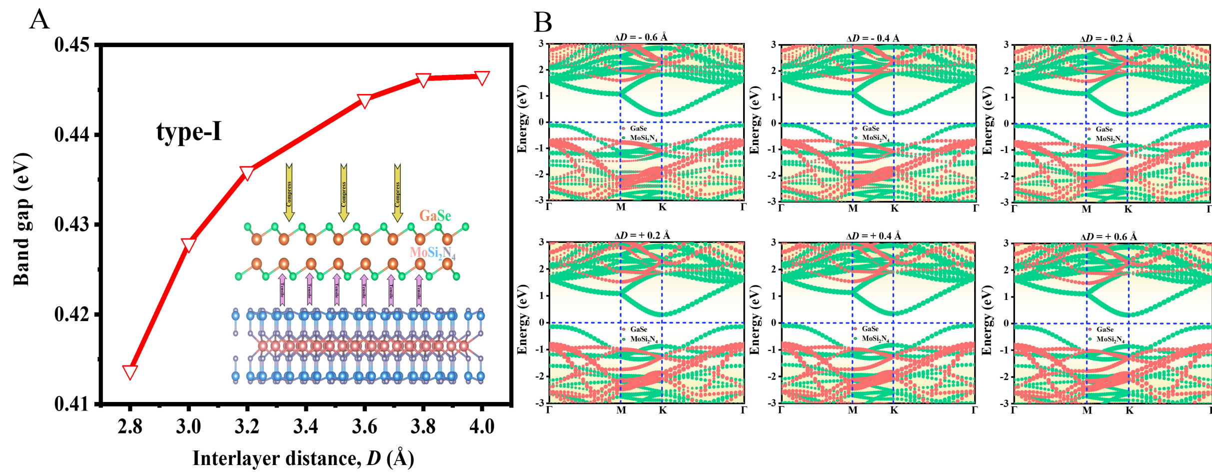

Figure 6. (A) GaSe/$MoSi_2N_4$ vdWH bandgap variation with interlayer distance. The illustration is a schematic model of applying strain in the z-direction; (B) GaSe/$MoSi_2N_4$ vdWH band structure at different interlayer distances. vdWHs: van der Waals heterostructures; GaSe: Gallium selenide.

rises from 2.8 Å to 4.0 Å. By studying the band structure in Figure 6B, the underlying mechanism of GaSe/$MoSi_2N_4$ vdWHs bandgap variation under strain engineering can be described. By applying tensile strain (i.e., as D increases), the CBM and VBM of GaSe/$MoSi_2N_4$ vdWHs barely change, indicating that the bandgap remains unchanged, and the type-I band structure is also retained in GaSe/$MoSi_2N_4$ vdWHs. Under compressive strain, as D (3.4 Å) decreases to 2.8 Å, VBM and CBM in the red GaSe layer shift slightly upward, while VBM and CBM in the green $MoSi_2N_4$ layer hardly change and still maintain the band structure of type-I. These results show that there is no change in b-a from type-I to type-II by changing the interlayer distance.

Furthermore, the effect of in-plane strain on the electronic structure of GaSe/$MoSi_2N_4$ vdWHs is considered. The in-plane strain is defined as:

$$\varepsilon = \left[\frac{a - a_s}{a}\right] \times 100 \quad (3)$$

Here, a and a_S denote the lattice parameters of GaSe/$MoSi_2N_4$ vdWHs without and in-plane strain, respectively. The bandgap change of GaSe/$MoSi_2N_4$ vdWHs is shown in Figure 7A. We found that the bandgap of GaSe/$MoSi_2N_4$ vdWHs decreased due to the in-plane strain. The bandgap of GaSe/$MoSi_2N_4$ vdWHs is reduced to 0.24 eV when ε = +6% tensile strain is applied. By applying in-plane compression strain, the bandgap of GaSe/$MoSi_2N_4$ vdWHs increases gradually and reaches a maximum value of 0.88 eV at -6% in-plane compression strain. Even more intriguingly, we found that the in-plane strain includes not only a change in the GaSe/$MoSi_2N_4$ vdWHs bandgap, but also a shift between type-I and type-II b-a. To better understand the underlying mechanism of the above behavior, we further mapped the projected band structure of GaSe/$MoSi_2N_4$ vdWHs under different tensile and compressive strains, as shown in Figure 7B. With the compression strain ε = -2% to -6% in the applied plane, the CBM of the $MoSi_2N_4$ layer shifts upward, causing it to move away from the Fermi level (E_F), and the VBM position hardly changes, while the VBM and CBM of GaSe layers are close to the E_F. In this instance, GaSe/$MoSi_2N_4$ vdWHs exhibit a type-I b-a; both VBM and CBM are contributed by the $MoSi_2N_4$ layer and have an indirect bandgap semiconductor at the Γ, K point. Besides, the CBM of the $MoSi_2N_4$ layer moves downward towards the E_F, VBM moves downward away from the E_F, and both VBM and CBM of the GaSe layer move closer to the E_F with the in-plane tensile strain ε = +2% to +4%. In this case, GaSe/$MoSi_2N_4$ vdWHs exhibit a type-I b-a; both

 Jiang *et al. Microstructures* **2025**, *5*, 2025009 | https://dx.doi.org/10.20517/microstructures.2023.100

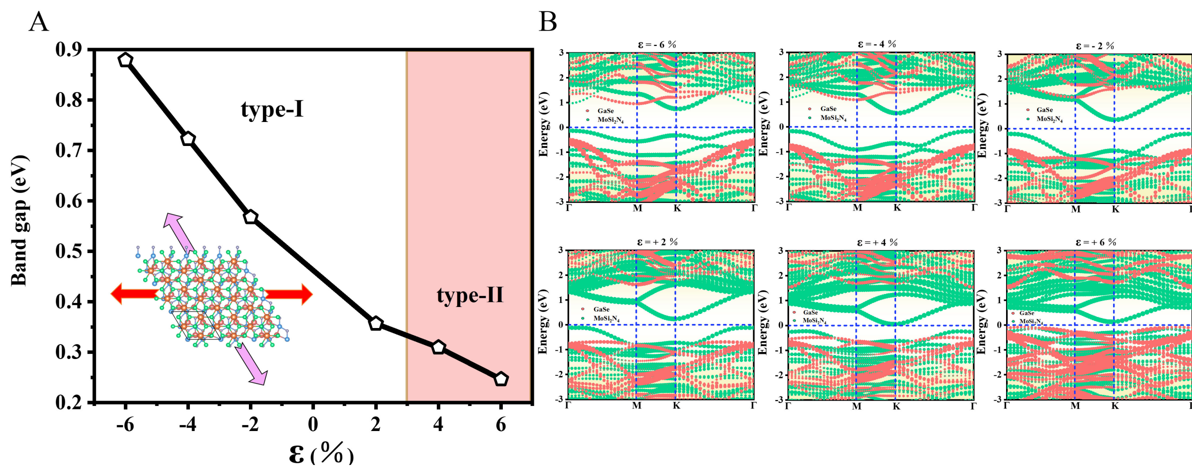

Figure 7. (A) Variation of GaSe/$MoSi_2N_4$ vdWH bandgap with in-plane strain. The illustration is a schematic model of the applied in-plane strain; (B) Projected band structure of GaSe/$MoSi_2N_4$ vdWHs under in-plane strain of ε = -6%, -4%, -2%, +2%, +4%, +6%. vdWHs: van der Waals heterostructures; GaSe: Gallium selenide.

VBM and CBM are contributed by the $MoSi_2N_4$ layer and have an indirect bandgap semiconductor at the K, Γ point. More interestingly, when ε = +4%, we find that GaSe layer CBM changes from the original M point to Γ point, and VBM changes from the original Γ point to between M and Γ point. Noteworthy is the fact that the positions of CBM and VBM in the $MoSi_2N_4$ layer almost do not change with the in-plane tensile strain ε reaching +6%, while the VBM in the GaSe layer moves upward to the E_F and the VBM in the GaSe layer is higher than that in $MoSi_2N_4$ layer. The results show that there is a shift from type-I to type-II b-a in GaSe/$MoSi_2N_4$ vdWHs. According to the above results, in-plane strain can effectively regulate the b-a and electronic structure of GaSe/$MoSi_2N_4$ vdWHs, which will be conducive to the design of high-efficiency nanoscale devices.

The use of external vertical electric fields presents an additional efficacious approach for controlling the electronic structure of 2D materials and vdWHs. We explore the effects of an electric field applied perpendicular to the GaSe/$MoSi_2N_4$ vdWHs, as shown in Figure 8A. The direction of the electric field from $MoSi_2N_4$ towards the GaSe layer is defined as the positive direction (from bottom to top in the illustration). In Figure 8A, we find that the application of a negative electric field hardly causes a large change in the bandgap of GaSe/$MoSi_2N_4$ vdWHs. However, when a positive electric field is applied, we can observe that a decrease in the bandgap is observed as the field is intensified. When a positive electric field greater than +0.2 V/Å is applied, the bandgap of GaSe/$MoSi_2N_4$ vdWHs decreases to zero, resulting in a transition from semiconductor to metal (Supplementary Figure 3 describes the projected band structure of GaSe/$MoSi_2N_4$ vdWHs at an electric field of +0.3 V/Å). Interestingly, we found that applying an external electric field included not only a change in the GaSe/$MoSi_2N_4$ vdWHs bandgap, but also a shift between type-I and type-II b-a. In order to better understand the underlying mechanism of the above behavior, the projected band structure of GaSe/$MoSi_2N_4$ vdWHs was also plotted to describe the bandgap trend, as shown in Figure 8B. With the application of a negative electric field of - 0.1 to - 0.2 V/Å, the position of CBM and VBM in the $MoSi_2N_4$ layer hardly changes, while the GaSe layer CBM moves downward towards the E_F and VBM moves downward away from the E_F. In this case, the CBM of the GaSe layer in vdWHs is above the CBM of $MoSi_2N_4$, and the VBM of the GaSe layer is below the VBM of $MoSi_2N_4$, so there is a type-I b-a (where both VBM and CBM are contributed by the $MoSi_2N_4$ layer). On the other hand, with the application of a positive electric field of +0.1 to +0.2 V/Å, the CBM and VBM of the $MoSi_2N_4$ layer move downward to the lower energy level, and the VBM and CBM of the GaSe layer move upward to the higher energy level. In

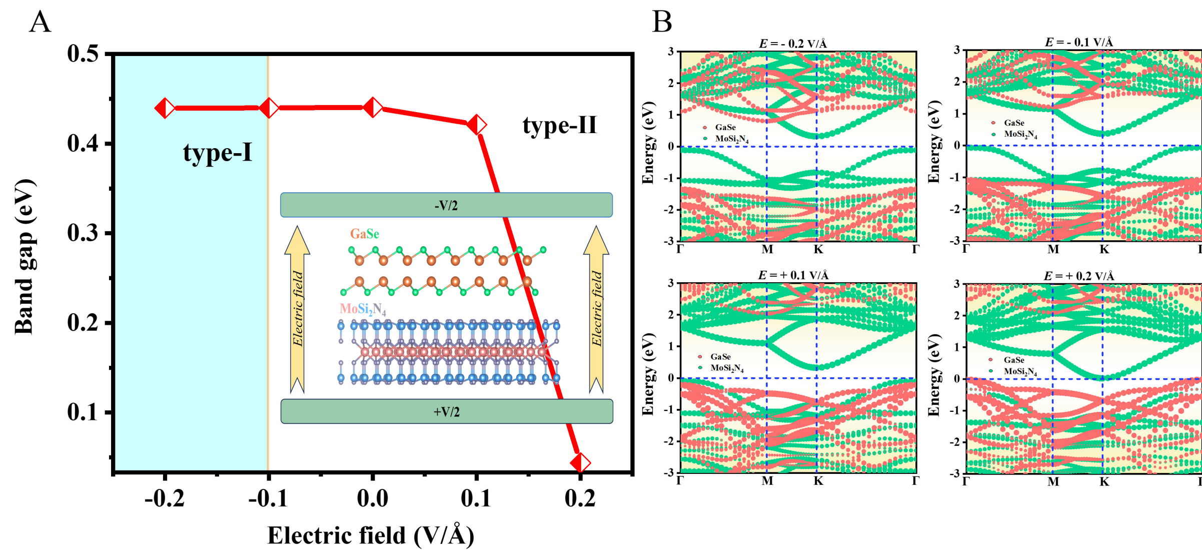

Figure 8. (A) Variation of bandgap of GaSe/$MoSi_2N_4$ vdWHs with electric field. The illustration is a diagram of applying an electric field along the vdWHs z-direction; (B) Projected band structure of GaSe/$MoSi_2N_4$ vdWHs under different electric field intensities. vdWHs: van der Waals heterostructures; GaSe: Gallium selenide.

this case, both CBM and VBM of the GaSe layer in vdWHs are above $MoSi_2N_4$, so it appears as a type-II b-a (where CBM is contributed by $MoSi_2N_4$ layer and VBM is contributed by GaSe layer). These discoveries imply that the electric field is an effective regulating knob for the type of b-a between type-I and type-II.

CONCLUSIONS

In a word, we investigate the structural characteristics and electronic properties of GaSe/$MoSi_2N_4$ vdWHs by first-principles calculations and explore the interlayer distance, in-plane strain, adjustable electronic structure and band alignment under external electric fields. The results show that the heterostructure exhibits stability at standard room temperature and possesses characteristics of an indirect bandgap semiconductor. Notably, we observed that both CBM and VBM of GaSe/$MoSi_2N_4$ vdWHs are derived from monolayer $MoSi_2N_4$, thus forming a type-I b-a. Furthermore, by applying in-plane strain, the external vertical electric field can separate the band edges of GaSe/$MoSi_2N_4$ vdWHs from the GaSe and $MoSi_2N_4$ layers, leading to a shift from type-I to type-II b-a types. Our results reveal the great potential of GaSe/$MoSi_2N_4$ vdWHs as a tunable material in optoelectronic applications.

DECLARATIONS

Acknowledgments

The authors would like to express their gratitude to Prof. Qu, X. and Prof. Liu, H. for their valuable guidance and technical support in two-dimensional heterostructures.

Authors' contributions

The conception and design of the work: Jiang, H.; Zhu, X.; Qu, X.
Data acquisition and analysis:Jiang, H.; Zhu, X.
Writing - original draft: Jiang, H.; Zhu, X.
Investigation: Zhu,X.; Jiang, H.; Wang, D.; Yang, L.; Liu, Y.
Data interpretation of data: Jiang, H.; Zhu, X.; Qu, X.; Liu, H.

Writing - review and editing: Qu, X.; Liu, H.

Availability of data and materials

The data that support the findings of this study are available from the corresponding author upon reasonable request.

Financial support and sponsorship

This study was financially supported by the Program for the National Natural Science Foundation of China (Grant No. 12204194), the Program for the Development of Science and Technology of Jilin Province (Grant Nos. YDZJ202101ZYTS065, 20210509050RQ, JJKH20220423KJ, 20220203021SF), the Open Project of State Key Laboratory of Superhard Materials, Jilin University (Grant No. 201908, 202306), and the Program for the Industrial Technology and Development of Jilin Province Development and Reform Commission (Item No. 2023C44-4).

Conflicts of interest

All authors declared that there are no conflicts of interest.

Ethical approval and consent to participate

Not applicable.

Consent for publication

Not applicable.

Copyright

© The Author(s) 2025.

REFERENCES

1. Geim, A. K.; Grigorieva, I. V. Van der Waals heterostructures. *Nature* **2013**, *499*, 419-25. DOI
2. Liu, Y.; Weiss, N. O.; Duan, X.; Cheng, H.; Huang, Y.; Duan, X. Van der Waals heterostructures and devices. *Nat. Rev. Mater.* **2016**, *1*, 16042. DOI
3. Novoselov, K. S.; Mishchenko, A.; Carvalho, A.; Castro, N. A. H. 2D materials and van der Waals heterostructures. *Science* **2016**, *353*, aac9439. DOI
4. Jin, C.; Ma, E. Y.; Karni, O.; Regan, E. C.; Wang, F.; Heinz, T. F. Ultrafast dynamics in van der Waals heterostructures. *Nat. Nanotechnol.* **2018**, *13*, 994-1003. DOI
5. Wang, Z.; Xu, B.; Pei, S.; et al. Recent progress in 2D van der Waals heterostructures: fabrication, properties, and applications. *Sci. China. Inf. Sci.* **2022**, *65*, 3432. DOI
6. He, J.; Wang, C.; Zhou, B.; Zhao, Y.; Tao, L.; Zhang, H. 2D van der Waals heterostructures: processing, optical properties and applications in ultrafast photonics. *Mater. Horiz.* **2020**, *7*, 2903-21. DOI
7. Liao, W.; Huang, Y.; Wang, H.; Zhang, H. Van der Waals heterostructures for optoelectronics: progress and prospects. *Appl. Mater. Today.* **2019**, *16*, 435-55. DOI
8. Liang, S. J.; Cheng, B.; Cui, X.; Miao, F. Van der Waals heterostructures for high-performance device applications: challenges and opportunities. *Adv. Mater.* **2020**, *32*, e1903800. DOI
9. Li, C.; Zhou, P.; Zhang, D. W. Devices and applications of van der Waals heterostructures. *J. Semicond.* **2017**, *38*, 031005. DOI
10. Liu, C. H.; Clark, G.; Fryett, T.; et al. Nanocavity integrated van der Waals heterostructure light-emitting tunneling diode. *Nano. Lett.* **2017**, *17*, 200-5. DOI
11. Binder, J.; Withers, F.; Molas, M. R.; et al. Sub-bandgap voltage electroluminescence and magneto-oscillations in a WSe_2 light-emitting van der Waals heterostructure. *Nano. Lett.* **2017**, *17*, 1425-30. DOI
12. Yan, R.; Fathipour, S.; Han, Y.; et al. Esaki diodes in van der Waals heterojunctions with broken-gap energy band alignment. *Nano. Lett.* **2015**, *15*, 5791-8. DOI
13. Özçelik, V. O.; Azadani, J. G.; Yang, C.; Koester, S. J.; Low, T. Band alignment of two-dimensional semiconductors for designing heterostructures with momentum space matching. *Phys. Rev. B.* **2016**, 94. DOI
14. Massicotte, M.; Schmidt, P.; Vialla, F.; et al. Picosecond photoresponse in van der Waals heterostructures. *Nat. Nanotechnol.* **2016**, *11*, 42-6. DOI

15. Lin, Y. C.; Ghosh, R. K.; Addou, R.; et al. Atomically thin resonant tunnel diodes built from synthetic van der Waals heterostructures. *Nat. Commun.* **2015**, *6*, 7311. DOI PubMed PMC
16. Zhou, Y.; Nie, Y.; Liu, Y.; et al. Epitaxy and photoresponse of two-dimensional GaSe crystals on flexible transparent mica sheets. *ACS. Nano.* **2014**, *8*, 1485-90. DOI
17. Hu, P.; Wen, Z.; Wang, L.; Tan, P.; Xiao, K. Synthesis of few-layer GaSe nanosheets for high performance photodetectors. *ACS. Nano.* **2012**, *6*, 5988-94. DOI
18. Lei, S.; Ge, L.; Liu, Z.; et al. Synthesis and photoresponse of large GaSe atomic layers. *Nano. Lett.* **2013**, *13*, 2777-81. DOI
19. Late, D. J.; Liu, B.; Luo, J.; et al. GaS and GaSe ultrathin layer transistors. *Adv. Mater.* **2012**, *24*, 3549-54. DOI
20. Zhuang, H. L.; Hennig, R. G. Single-layer group-III monochalcogenide photocatalysts for water splitting. *Chem. Mater.* **2013**, *25*, 3232-8. DOI
21. Zappia, M. I.; Bianca, G.; Bellani, S.; et al. Solution-processed GaSe nanoflake-based films for photoelectrochemical water splitting and photoelectrochemical-type photodetectors. *Adv. Funct. Mater.* **2020**, *30*, 1909572. DOI
22. Ben, A. Z.; Pierucci, D.; Henck, H.; et al. Tunable quasiparticle band gap in few-layer GaSe/graphene van der Waals heterostructures. *Phys. Rev. B.* **2017**, *96*, 035407. DOI
23. Jung, C. S.; Shojaei, F.; Park, K.; et al. Red-to-ultraviolet emission tuning of two-dimensional gallium sulfide/selenide. *ACS. Nano.* **2015**, *9*, 9585-93. DOI
24. Cui, Y.; Peng, L.; Sun, L.; Qian, Q.; Huang, Y. Two-dimensional few-layer group-III metal monochalcogenides as effective photocatalysts for overall water splitting in the visible range. *J. Mater. Chem. A.* **2018**, *6*, 22768-77. DOI
25. Allakhverdiev, K. R.; Yetis, M. Ö.; Özbek, S.; Baykara, T. K.; Salaev, E. Y. Effective nonlinear GaSe crystal. Optical properties and applications. *Laser. Phys.* **2009**, *19*, 1092-104. DOI
26. Leontie, L.; Evtodiev, I.; Nedeff, V.; Stamate, M.; Caraman, M. Photoelectric properties of Bi_2O_3/GaSe heterojunctions. *Appl. Physs. Lett.* **2009**, *94*, 071903. DOI
27. Xia, C.; Li, J. Recent advances in optoelectronic properties and applications of two-dimensional metal chalcogenides. *J. Semicond.* **2016**, *37*, 051001. DOI
28. Zhang, X.; Wang, S.; Wan, G.; Zhang, Y.; Huang, M.; Yi, L. Transient reflectivity measurement of photocarrier dynamics in GaSe thin films. *Appl. Phys. B.* **2017**, *123*, 1-7. DOI
29. Liu, S.; Mahony, T. S.; Bender, D. A.; Sinclair, M. B.; Brener, I. Mid-infrared time-domain spectroscopy system with carrier-envelope phase stabilization. *Appl. Phys. Lett.* **2013**, *103*, 181111. DOI
30. Zhang, C. J.; Park, S. H.; Ronan, O.; et al. Enabling flexible heterostructures for Li-ion battery anodes based on nanotube and liquid-phase exfoliated 2D gallium chalcogenide nanosheet colloidal solutions. *Small* **2017**, *13*, 1701677. DOI
31. Hong, Y. L.; Liu, Z.; Wang, L.; et al. Chemical vapor deposition of layered two-dimensional $MoSi_2N_4$ materials. *Science* **2020**, *369*, 670-4. DOI
32. Bafekry, A.; Faraji, M.; Fadlallah, M. M.; et al. Tunable electronic and magnetic properties of $MoSi_2$N4 monolayer via vacancy defects, atomic adsorption and atomic doping. *Appl. Surf. Sci.* **2021**, *559*, 149862. DOI
33. Guo, X.; Guo, S. Tuning transport coefficients of monolayer $MoSi_2N_4$ with biaxial strain*. *Chinese. Phys. B.* **2021**, *30*, 067102. DOI
34. Jian, C.; Ma, X.; Zhang, J.; Yong, X. Strained $MoSi_2N_4$ monolayers with excellent solar energy absorption and carrier transport properties. *J. Phys. Chem. C.* **2021**, *125*, 15185-93. DOI
35. Pham, K. D.; Nguyen, C. Q.; Nguyen, C. V.; Cuong, P. V.; Hieu, N. V. Two-dimensional van der Waals graphene/transition metal nitride heterostructures as promising high-performance nanodevices. *New. J. Chem.* **2021**, *45*, 5509-16. DOI
36. Cao, L.; Zhou, G.; Wang, Q.; Ang, L. K.; Ang, Y. S. Two-dimensional van der Waals electrical contact to monolayer $MoSi_2N_4$. *Appl. Phys. Lett.* **2021**, *118*, 013106. DOI
37. Bafekry, A.; Faraji, M.; Abdollahzadeh, Z. A.; et al. A van der Waals heterostructure of MoS_2/$MoSi_2N_4$: a first-principles study. *New. J. Chem.* **2021**, *45*, 8291-6. DOI
38. Cai, X.; Zhang, Z.; Zhu, Y.; et al. A two-dimensional $MoSe_2$/$MoSi_2N_4$ van der Waals heterostructure with high carrier mobility and diversified regulation of its electronic properties. *J. Mater. Chem. C.* **2021**, *9*, 10073-83. DOI
39. Wang, Q.; Cao, L.; Liang, S.; et al. Efficient ohmic contacts and built-in atomic sublayer protection in $MoSi_2N_4$ and WSi_2N_4 monolayers. *npj. 2D. Mater. Appl.* **2021**, *5*, 71. DOI
40. Cohen, A. J.; Mori-Sánchez, P.; Yang, W. Challenges for density functional theory. *Chem. Rev.* **2012**, *112*, 289-320. DOI PubMed
41. Allouche, A. R. Gabedit--a graphical user interface for computational chemistry softwares. *J. Comput. Chem.* **2011**, *32*, 174-82. DOI PubMed
42. Blöchl, P. E. Projector augmented-wave method. *Phys. Rev. B.* **1994**, *50*, 17953-79. DOI
43. Momma, K.; Izumi, F. *VESTA 3* for three-dimensional visualization of crystal, volumetric and morphology data. *J. Appl. Crystallogr.* **2011**, *44*, 1272-6. DOI
44. Perdew, J. P.; Burke, K.; Ernzerhof, M. Generalized gradient approximation made simple. *Phys. Rev. Lett.* **1996**, *77*, 3865-8. DOI PubMed
45. Paier, J.; Hirschl, R.; Marsman, M.; Kresse, G. The perdew-burke-ernzerhof exchange-correlation functional applied to the G2-1 test set using a plane-wave basis set. *J. Chem. Phys.* **2005**, *122*, 234102. DOI
46. Heyd, J.; Scuseria, G. E.; Ernzerhof, M. Hybrid functionals based on a screened coulomb potential. *J. Chem. Phys.* **2003**, *118*, 8207-15. DOI

47. Togo, A.; Tanaka, I. First principles phonon calculations in materials science. *Scripta. Mater.* **2015**, *108*, 1-5. DOI
48. Grzonka, J.; Claro, M. S.; Molina□sánchez, A.; Sadewasser, S.; Ferreira, P. J. Novel polymorph of GaSe. *Adv. Funct. Mater.* **2021**, *31*, 2104965. DOI
49. Born, M.; Huang, K.; Lax, M. Dynamical theory of crystal lattices. *Am. J. Phys.* **1955**, *23*, 474. DOI
50. Mouhat, F.; Coudert, F. Necessary and sufficient elastic stability conditions in various crystal systems. *Phys. Rev. B.* **2014**, *90*, 224104. DOI
51. Zhang, W. X.; Yin, Y.; He, C. Spontaneous enhanced visible-light-driven photocatalytic water splitting on novel type-II GaSe/CN and Ga_2SSe/CN vdW heterostructures. *J. Phys. Chem. Lett.* **2021**, *12*, 5064-75. DOI
52. He, C.; Liang, Y.; Zhang, W. Constructing a novel metal-free g-C_3N_4/g-CN vdW heterostructure with enhanced visible-light-driven photocatalytic activity for water splitting. *Appl. Surf. Sci.* **2021**, *553*, 149550. DOI
53. Yankowitz, M.; Watanabe, K.; Taniguchi, T.; San-Jose, P.; LeRoy, B. J. Pressure-induced commensurate stacking of graphene on boron nitride. *Nat. Commun.* **2016**, *7*, 13168. DOI PubMed PMC
54. Tongay, S.; Fan, W.; Kang, J.; et al. Tuning interlayer coupling in large-area heterostructures with CVD-grown MoS_2 and WS_2 monolayers. *Nano. Lett.* **2014**, *14*, 3185-90. DOI